Contents lists available at SciVerse ScienceDirect

Chemical Engineering Research and Design

journal homepage: www.elsevier.com/locate/cherd

Actinides oxalate precipitation in emulsion modeling: From the drop scale to the industrial process

Sophie Charton[a,*], Amine Kacem[a], Abdenour Amokrane[a,b], Gilles Borda[a], François Puel[b], Jean-Paul Klein[b]

[a] CEA, DEN, DTEC, SGCS, F-30207 Bagnols-sur-Cèze, France

[b] Université de Lyon, Université Lyon 1, CNRS, CPE Lyon, UMR 5007, Laboratoire d'Automatique et de Génie des Procédés (LAGEP), 43 Bd du 11 Novembre 1918, F-69622 Villeurbanne, France

ABSTRACT

An original process of actinides coprecipitation based on pulsed flow column is studied. The novelty of this process lies in the confinement of the aqueous reagents in separated droplets, dispersed in an inert organic phase (W/O emulsion). Precipitation occurs inside drops when they coalesce. Besides the implementation of well-known technologies of the nuclear industry, this precipitation in emulsion process is particularly convenient for the control of supersaturation, and ensures the sticky precipitates' confinement within drops, thereby limiting the fouling risk and its adverse consequences on productivity and safety.

A thorough understanding of the precipitation mechanisms and their interactions with the hydrodynamic conditions prevailing around and inside the drops is essential for the process optimization. In this context, numerical simulations were conducted, accompanying experiments, to study the process sensitivity. Different levels were considered in the modeling task, going from the emulsion behavior inside the column, to the reagents mixing and precipitation within the drops.

Regarding the drop scale, on which we focus in this paper, preliminary static and dynamic observations revealed a stage of mixing of the reagents, followed by a progressive concentration of particles at the drop center leading to their agglomeration. In the modeling three configurations of the reagents' mixing were therefore considered relatively to the Hill vortices experimentally noticed. CFD simulations allowed calculating possible mean supersaturation profiles in the drop. Two simplified models were proposed to simulate the precipitation inside the drops. Based on the population balance modeling framework, they consider primary nucleation and growth mechanisms and take into consideration either instantaneous or progressive mixing of the reagents. These simplified models were validated with CFD + PBM simulations. Based on the drop scale simulations, process modeling has been discussed.

Keywords: Precipitation in emulsion processes; Population balance modeling; Multiscale modeling; Nuclear fuel reprocessing

1. Introduction

Oxalic acid precipitation is used in the nuclear fuel treatment industry to recover selected actinides dissolved in nitric acid media. This operation is currently processed in a vortex flow apparatus (Auchapt and Ferlay, 1983), which size and capacity are limited, to mitigate the risk of criticality. In order to manufacture new compositions of nuclear fuel and/or transmutation targets, an alternative to the current method of reprocessing spent nuclear fuel, would be to co-extract chosen actinides and then to co-precipitate them in a single step.

The production of such a co-precipitate solid would require the development of a specific apparatus, either in order to increase the production rates, the latter being significantly enhanced by the joint precipitation of uranium and minor actinides for new nuclear fuel production, or to process high

* *Corresponding author*. Tel.: +33 466796229.
E-mail address: sophie.charton@cea.fr (S. Charton).
Received 27 July 2012; Received in revised form 24 January 2013; Accepted 1 February 2013
0263-8762/$ – see front matter
http://dx.doi.org/10.1016/j.cherd.2013.02.001

activity elements for transmutation purpose. To this end, we are studying a new concept of oxalic precipitation process, based on the use of either a pulsed or a Taylor–Couette flow column (Borda et al., 2008).

In this process, an inert organic phase (Tetra Propylene Hydrogen TPH) is pumped from bottom to top in a closed circuit. Both reagents: the complexing agent (oxalic acid) and the cations to be precipitated (dissolved in nitric acid) are fed individually in the contactor, where they are immediately dispersed as droplets: (i) thanks to the complex flow around the column's internals, generated by the pulsation (pulsed column Nemri et al. (2012)), (ii) or due to the Taylor vortices (Taylor–Couette column). The droplets are moving countercurrently to the inert organic phase, down to the settler, where the organic, aqueous and solid phases separate, thus enabling the solid recovery by filtration. The principle of the process is depicted in Fig. 1 for the pulsed column. The novelty of this process lies in the confinement of the reagents in drops of aqueous phase dispersed in the inert organic phase as shown in Fig. 1.

This "in emulsion" process exhibits the double advantage of (i) implementing well-known technologies of the nuclear industry, and (ii) ensuring the confinement of the sticky precipitate in the organic diluent, thereby limiting the risk of contamination of the apparatus and its adverse consequences in terms of productivity, safety, etc. Moreover, contrary to conventional contactors where the precipitation process is strongly dependent on the position of the two feed lines, here the initial mixing of the reagents and reaction induction time are not directly influenced by the apparatus feed conditions.

Regarding pulsed column, the process feasibility was demonstrated in a wide range of flow-rates and chemical conditions. The apparatus, operating conditions and main results are described in (Borda et al., 2011). Feasibility was also demonstrated recently in Taylor–Couette configuration, for which a parametric study is under progress. For these production tests of Ce^{III}, Nd^{III} and mixed $U^{IV} + Ce^{III}$ precipitates, neodymium (Nd^{III}) and cerium (Ce^{III}) cations are used to simulate actinides, in order to reduce the inventory of radioactive materials involved in feasibility studies. The precipitation reaction of cerium in nitric media follows:

$$2Ce(NO_3)_3 + 3H_2C_2O_4 + 10H_2O \rightarrow Ce_2(C_2O_4)_3{\cdot}10H_2O + 6HNO_3 \quad (1)$$

Whatever the column technology, besides the classical chemical parameters known to influence supersaturation (pH, reagents ratio, etc.), purely hydrodynamic conditions were observed to have an effect on the produced solid properties, such as particle size distribution and particle habit, presumably due to the evolution of the emulsion properties. Indeed, the droplets' size, their residence time, collision frequencies, etc. are strongly related to the pulsation amplitude and frequency in the pulsed column (respectively the gap size and the rotor speed regarding the Taylor–Couette contactor).

Therefore, as for the vortex flow reactor today used in the fuel processing plant (Bertrand et al., 2012), a comprehensive modeling study of the interactions between the precipitation mechanisms and the hydrodynamic conditions prevailing around the droplets in the pulsed column has been undertaken. The methodology is transposable to the Taylor–Couette configuration. In this aim, CFD is used both at the column and at the drop scales independently. Indeed, contrary to usual emulsion crystallization processes, where the particles derive from solidification of the dispersed droplets (Davey et al., 1997; Khalil et al., 2012), where reagents are transferred from the continuous phase (Bandyopadhyaya et al., 1997), or where the crystallization occurs by a quasi-crystallization mechanism (Espitalier et al., 1997), in the studied process the continuous phase is totally inert. Its only role is to allow collisions between droplets, i.e. the actual reactors, whose coalescence initiates the reaction. Actually, despite the increased complexity of the modeling task, the decoupling of these two scales eliminates the influence of the column's feeding conditions on the nucleation process and the properties of the solid.

At the column level, the drop population behavior is considered in order to correlate their size distribution, residence times and collision frequency to the reactor operating conditions, such as column and packing geometry, amplitude and frequency of the pulsed flow, feed rates, etc. (Amokrane et al., 2012). Whereas at the drop scale, which is the object of this article, the reagents mixing within the drops, depending on their outer and initial conditions, and the resulting solid particles nucleation, growth and agglomeration processes are considered.

After examining the available precipitation data in Section 2, the methodology developed to model the processes occurring in the droplets is presented. The detailed description of the mixing process during the coalescence is not taken into account for the moment, however, preliminary experimental observations, supplemented by flow simulations, allowed us to simplify the problem in the framework of a chemical engineering approach, described in Section 3. To conclude, the extrapolation to the simulation of the precipitation in emulsion process, and its performances, is discussed in Section 4.

2. Precipitation data

The obvious required parameters, for precipitation modeling purpose, are the equilibrium data (product solubility) and kinetic data. Both types are empirically determined, and are therefore closely related to the thermodynamic description of the ionic media, and in particular the model used for calculating activity coefficients. Moreover, kinetic data are generally dependent on operating conditions (reactor type, injection point position, stirrer speed, etc.) as discussed Section 3.3.2. While it is already difficult to obtain reliable kinetic data, little data are available regarding either actinides oxalate precipitation and their nonradioactive stand-in:

- The uranium oxalate and the neodymium oxalate systems had been studied by Andrieu (1999) and more recently by Lalleman et al. (2012). Regarding the calculation of activity coefficients, and from there the calculation of solubility products, supersaturation values, and kinetic parameters, both works relied on the Bromley model (1973), which is valid for ionic strength up to $I = 6\,mol\,l^{-1}$.
- Cerium oxalate precipitation has, to our knowledge, not been investigated since the experimental work of Chang (1987) in SRNL. The study was purely empirical and the given correlation results from non-linear regression of experimental data.

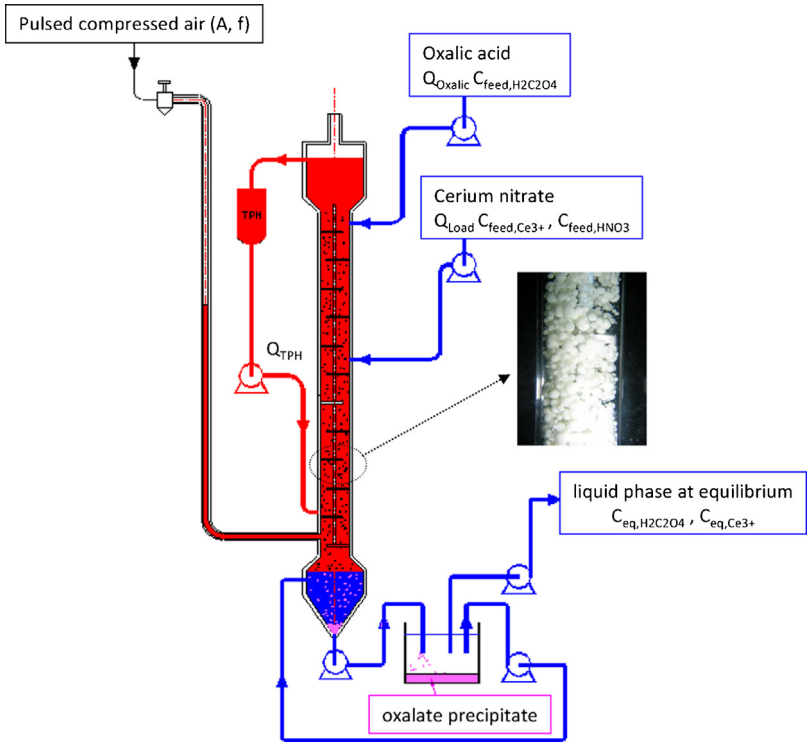

Fig. 1 – Principle of the pulsed column contactor operating as a continuous oxalate precipitation reactor (Borda et al., 2011). The picture shows the droplets enclosing the cerium oxalate precipitate during the column functioning.

In the present study, activity coefficients were calculated using the Davies modification of the Debye–Hückel model (Davies, 1938). Indeed, within the studied process, ionic strength within the drops remained moderate (see Table 1). This model has been commonly used in rare earth oxalate solubility studies (Chung et al., 1998). Moreover, it is simpler to implement in simulation code than the Bromley theory, for which the oxalate contribution is not known to date.

The Davies model is written as follow:

$$\log\ \gamma_i = \frac{-0.509 \times z_i^2 \times \sqrt{I}}{1 + 0.329.10^8 \times a_i \times \sqrt{I}} - 0.1 \times I \quad (2)$$

$$I = \frac{1}{2}\sum_i C_i z_i^2 \quad (3)$$

where z_i is the charge number of ion i, C_i its concentration in the solution, a_i a ion size constant, and I is the ionic strength of the solution.

Considering reaction (1) for Cerium oxalate precipitation, and assuming total dissociation of both nitric and oxalic acids (Lalleman et al., 2012), the mean activity coefficient is expressed by Eq. (4):

$$\overline{\gamma} = \left(\prod_i \gamma_i^{\nu_i}\right)^{1/\sum_i \nu_i} = \left(\gamma^2_{Ce^{3+}} \times \gamma^6_{NO_3^-} \times \gamma^6_{H^+} \times \gamma^3_{C_2O_4^{2-}}\right)^{1/17} \quad (4)$$

Table 1 – Typical operating conditions for Cerium oxalate precipitation in emulsion.

	Feed	Equilibrium
Ce^{3+}	24 g/l	20 mg/l
HNO_3	1.5 N	0.92 N
$H_2C_2O_4$	0.7 mol l^{-1}	0.25 mol l^{-1}
I (mol l^{-1})	2.17	0.51

The supersaturation ratio is given by:

$$s = \overline{\gamma}\left(\frac{C^2_{Ce^{3+}} \times C^3_{C_2O_4^{2-}}}{K_{SP}}\right)^{1/5} \quad (5)$$

where K_{SP} is the Cerium oxalate solubility product, defined in accordance with Andrieu (1999):

$$K_{SP} = \overline{\gamma}^5_{eq} \times C^2_{eq,Ce^{3+}} \times C^3_{eq,C_2O_4^{2-}} \quad (6)$$

The value of K_{SP} is calculated using the equilibrium concentrations achieved in the settler of the pulsed column (Borda et al., 2011) and reported in Table 1.

Regarding kinetic data, the general expression for the nucleation rate is of the type:

$$R_N = A_N \times \exp\left(\frac{-B_N}{(\ln s)^2}\right) \quad (7)$$

where A_N and B_N are constants and where s is the supersaturation ratio defined by Eq. (5).

The growth rate (G in m s^{-1}) is assumed to be independent of particle size and is expressed by:

$$G = \frac{\partial L}{\partial t} = G_0 \times (C - C_{eq}) \quad (8)$$

where L is the characteristic size of the particle (m), C and C_{eq} the Ce^{3+} concentration respectively in the drop and at equilibrium, given in Table 1, and G_0 is a constant.

Given the lack of kinetic data regarding cerium oxalate precipitation (except from the work of Chang (1987) from which it is not possible to derive the values of A_N and B_N), we decided for the modeling purpose to consider only neodymium oxalate kinetic parameters (see Table 2).

Table 2 – Kinetic parameters used for the simulations.

A_N	6.3×10^{19} ($m^{-3}\,s^{-1}$)
B_N	201
G_0	6.3×10^{-9} (m s)

Indeed, as observed by Borda et al. (2011), cerium and neodymium oxalates precipitation experiments are leading to similar results: the average particles size ranges from 15 to 30 μm (although Nd oxalate particles are slightly smaller than the Ce ones, in agreement with their smaller solubility), and the analysis of the outlet flux composition indicates that the precipitation reaction is total.

3. Study and modeling of the reaction process

3.1. *Preliminary experimental study*

Prior to the modeling approach, drop scale experiments were conducted in order to the study the relevant phenomena taking place within a newly coalesced droplet, possibly subjected to hydrodynamic conditions similar to those prevailing in a pulsed column. Observations made during and after collision of a cerium nitrate drop with an other one containing oxalic acid in TPH media, helped us to identify the main stages of the precipitation process. All experiments were conducted according to Table 1 feed conditions.

The small quantities of reagents involved in these preliminary experiments, did not allowed the analysis of the solid properties. The latter, already in small quantity, was generally sticking to the support plate at the end of experiments.

Regarding the reaction progress in static configuration, whatever the volumes and compositions of the two fused droplets, the same behavior was observed. First of all, no mixing occurred during the early stages of film drainage and the overall shape evolution (Pontisso et al., 2011). Moreover, a thin veil of solid particles appeared immediately after the fusion of the two drops, as attested by high-speed camera observations (Fig. 2, left). After coalescence, cerium nitrate, which exhibits the higher density, was always located in the lower part of the drop, whereas oxalic acid remained at the top, still separated by the veil of solid particles (Fig. 2, right). In the static conditions of the sessile drop tests, the veil was observed to limit the mass transfer between the two zones. After a while, the particles of the veil aggregated in clusters, which settled gradually on the support plate (Medal et al., 2010).

A second series of experiments was performed under dynamic conditions by maintaining the fused droplet in a TPH stream, instead of being immobilized on the support plate (Picard, 2012). In this configuration, the TPH flow-rate was adjusted in order to achieve a slip velocity typical of a pulsed column i.e. $u_{ax} = 0.1\,m\,s^{-1}$ (Amokrane et al., 2012). Although the device was not properly optimized for quantitative measurements, as in Groß-Hardt et al. (2008), intense agitation was observed within the moving drop. The particles gradually concentrated in the center of the drop where they can agglomerate (Medal et al., 2010). Only the smallest particles, not "bonded" in the central cluster, continued to circulate along the Hill vortices streamlines. A similar behavior was observed during the pulsed column functioning where the precipitates clusters gradually settled, while remaining confined in the drop.

3.2. *Mixing in a flowing drop: CFD approach*

Mixing plays a major role on precipitation process, and more generally on fast chemical reaction, as discussed by several authors (Torbacke and Rasmuson, 2001; Cameirão et al., 2008; Ståhl and Rasmuson, 2009). Computational fluid dynamics (CFD) is therefore frequently used to account for micromixing (Marchisio and Barresi, 2003), and even to quantify segregation in the reactor. Hence, in the case of an agglomeration-dominated system, Ilievski et al. (2001) have studied the separate influence of shear rate, which affects particles capture efficiency and aggregates rupture; and mixing, which affects particles transport and collision rate.

In order to investigate the mixing efficiency in the drops, suggested by the intense agitation observed during the dynamic experiments, CFD simulations were performed in a 2D frame, using the commercial software ANSYS-FLUENT©.

Given the water/TPH system properties, the 2–3 mm-diameter droplets flowing in the pulsed column are characterized by an Eötvös number ranging from 0.2 to 0.6, which is typical of droplets with a spherical shape (Clift et al., 1978).

The downward movement in the column frame is simulated by imposing a constant and unidirectional velocity, equal to the slip velocity u_{ax}, at the drop wall. This was implemented using the "translational imposed velocity" option available in the software boundary conditions panel. This kind of boundary condition indeed set the tangential velocity, u_θ all around the drop interface to $0 \leq u_\theta \leq u_{ax}$ from pole to equator. This velocity profile is in accordance with Saboni et al. (2004) results in the considered range of Re (Re ≤ 300) and with viscosity and density ratios closed to 1.

A sensitivity study to the mesh size was performed, based on the mixing kinetics. Five quadrangular grids, going from 2000 to 12,000 cells, were tested with a time step of 10^{-5} s, which is far below the characteristic times for diffusion and advective transport of the species. No significant variation of the mixing kinetics was observed above 8000 cells, which was therefore the retained value. The optimal drop mesh is shown in Fig. 3.

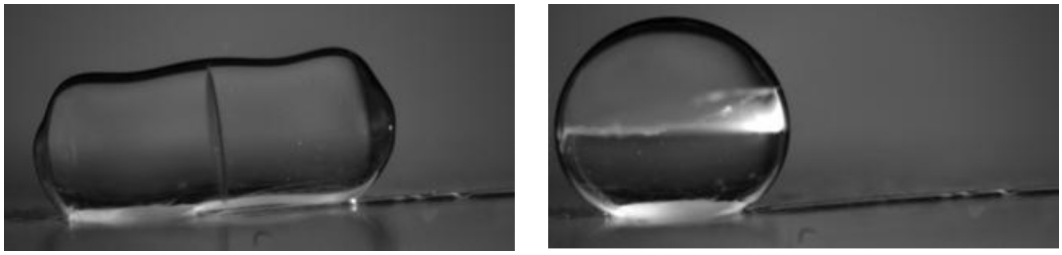

Fig. 2 – Coalescence of sessile drops immerged in TPH. Left: 20 ms after coalescence: oxalic acid (in the left part) and cerium nitrate (in the right part). Right: 60 s after coalescence: oxalic acid (in the upper part), cerium nitrate (in the lower part) and in between the veil of solid particles. NB: reaction ended in approx. 200 s (Pontisso et al., 2011).

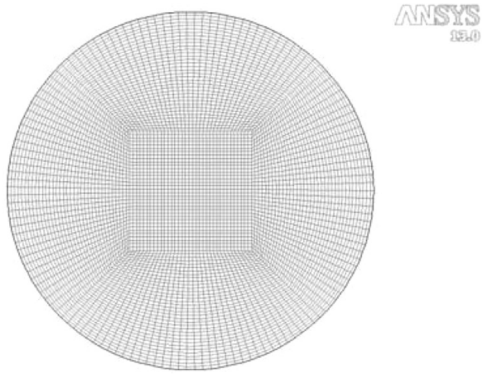

Fig. 3 – Droplet discretization for the CFD calculation (8000 cells).

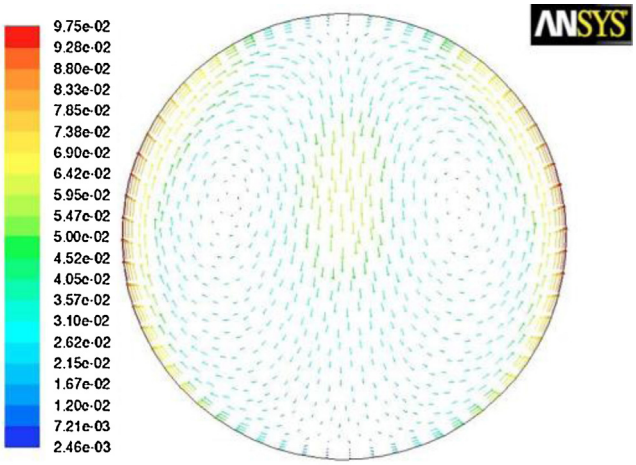

Fig. 4 – Simulated velocity vectors colored by velocity magnitude for $u_{ax} = 0.1\ m\ s^{-1}$.

Whereas species transport is solved, reaction is not taken into account at this stage. Eqs. (2)–(6) have been programmed in User Defined Functions in order to evaluate ionic strength and supersaturation for each cell of the computational domain.

As illustrated by Fig. 4, the translational movement of the droplet induces the development of Hill vortices, in agreement with the Hadamard–Rybcynski solution (Clift et al., 1978), and with experimental observations.

Three configurations were considered regarding the initial reagents distribution in the drop (see Fig. 5). The two first configurations derive from the sessile drop observations where each reagent seems to be stored in a separate hemisphere. The drop may be cut either perpendicularly (Config. 1) or in parallel (Config. 2), compared with the slip velocity vector direction. The third configuration studied (Config. 3), where one reagent is confined in the core of the drop, derives from Fang et al. (2011) micro-LIF observations of moving drop coalescence.

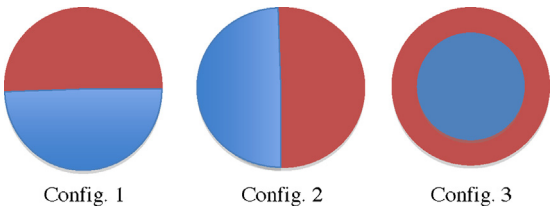

Fig. 5 – Schematic representation of the initial conditions considered for the coupled CFD + PBE simulation.

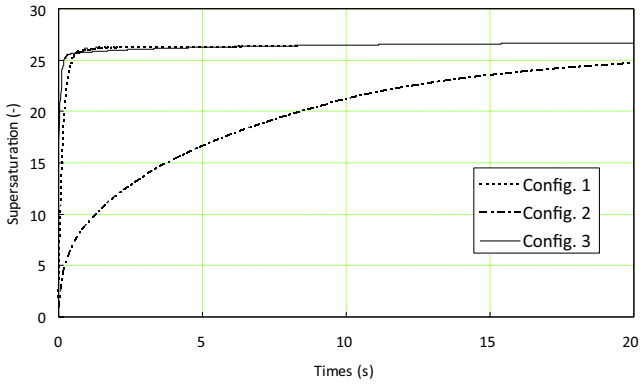

Fig. 6 – Initial conditions influence on the mixing kinetics.

The mean supersaturation evolutions predicted in each case are compared in Fig. 6. In the 1st and the 3rd configurations, homogeneous supersaturation is reached very quickly in the drop, and these two sets of initial conditions behave nearly identically. The contribution of the Hill vortices streamlines to the mixing process is clearly illustrated by the evolution of the supersaturation contours (Fig. 7). In the 2nd configuration conversely, when the concentration gradients are collinear to the velocity vectors in the drop core, the mean supersaturation exhibits a diffusion-like evolution and increases more slowly. In this configuration, the mixing of reagents by the Hill vortices is significantly less efficient (Fig. 7).

3.3. *Precipitation modeling inside a drop: a reaction engineering approach*

3.3.1. *Model equations and assumptions*

Based on the conclusion of the preliminary experiments, and the result of the CFD simulation regarding mixing, two simplified models were proposed in order to simulate the precipitation process at the drop scale.

The first one, suggested by the rapid and efficient mixing achieved in Config. 1 and Config. 3, assumes complete and instantaneous mixing of the reagents; the droplet is therefore considered as a closed continuously stirred tank reactor (CSTR).

The CSTR assumption is certainly not representative of the precipitation resulting from the collision and coalescence of two moving drops. It assumes that the reagents remain unmixed during the coalescence process, before being immediately and thoroughly mixed after coalescence. Although the experiments performed in static conditions mentioned in Section 3.1 confirmed the lack of mixing during the first stages of coalescence (as supported by high speed camera visualizations), these experiments revealed the early formation of a veil of solid particles limiting the mixing kinetics (Fig. 2, right). Moreover, besides the diffusion-like profile observed in Config. 2, CFD simulations have revealed in each case the early formation of a high supersaturation zone (Fig. 7, left), presumably conducive to the formation of a mass-transfer limiting veil.

A second model named Feed Diffusion Rate model (FDR) was therefore developed, where the CSTR, initially containing the cerium load, is fed, with a finite diffusion rate, by a "reservoir" containing the oxalic acid.

In each case, the model is based on the resolution of the transient population balance equation (PBE), Eq. (8), coupled

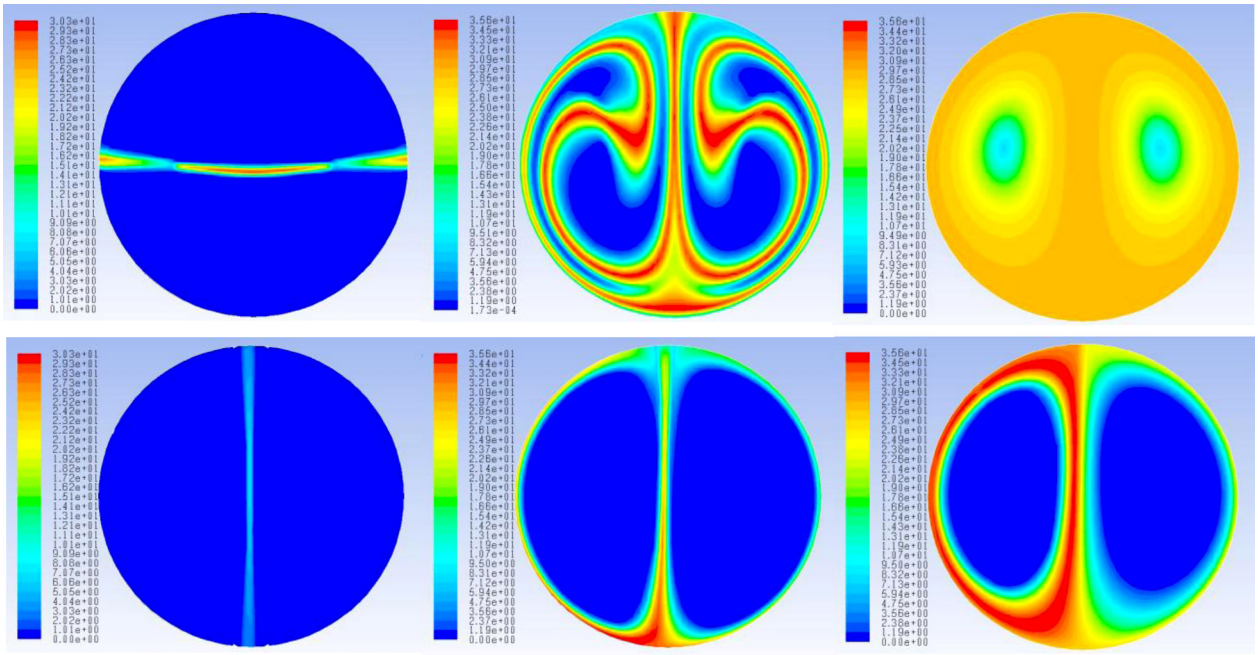

Fig. 7 – From left to right, supersaturation contours at 0.5 ms, 0.1 s and 1 s for Config. 1 (on top) and Config. 2 (at the bottom).

with the macroscopic balance equations for the species (Eq. (14a) or (14b)).

$$\frac{\partial\psi(L,t)}{\partial t} + G(t)\frac{\partial\psi(L,t)}{\partial L} = N(L,t) \tag{9}$$

In this equation, ψ (in $m^{-3}\,m^{-1}$) represents the number function distribution of the particles, G is the growth rate as defined by Eq. (7), and N (in $m^{-3}\,s^{-1}\,m^{-1}$) is the nucleation rate for particles of size L.

Agglomeration, breakage and dissolution phenomena are not taken into account in this first approach.

We chose to solve the PBE by a five-order finite volume scheme. Derivatives with respect to particle size are discretized by biased upwind finite differences on 5 points, by analogy with the work of Marcant (1992). Since first order finite difference methods are known to be unstable and subjected to numerical diffusion (Muhr et al., 1996), the accuracy of the five-order scheme chosen was checked using the size-independent growth test-case proposed by Qamar et al. (2007).

The source term is linearized in the nucleation class, according to the methodology proposed by Marcant (1992), thereby stabilizing the resolution algorithm. The nuclei critical size L_{crit} (and consequently the boundaries of the nucleation class) is evaluated as a function of supersaturation, according to the following reaction:

$$L_{crit} = \frac{1}{\ln(s)}\left(\frac{2M_S B_N}{\rho_S(\pi/6)\mathbf{N}}\right)^{1/3} \tag{10}$$

where ρ_S and M_S represent respectively the density (in $kg\,m^{-3}$) and molar weight (in $kg\,mol^{-1}$) of the solid phase and $\mathbf{N}$ is the Avogadro's number.

This source term is set to zero at all other nodes of the mesh.

$$N(L) = a_N L + b_N \tag{11}$$

The nucleation rate by size, N, is related to Eq. (6) by:

$$R_N = \int_{L=0}^{\infty} N(L)dL = \int_{L_{inf}}^{Lsup} N(L)dL \tag{12}$$

where L_{inf} and L_{sup} stands for the nucleation class boundary in the considered mesh.

The apparent (or macroscopic) reaction rate is expressed in $mol\,m^{-3}\,s^{-1}$ by:

$$\begin{aligned} r_{app} &= \underbrace{\frac{\rho_S}{M_S}\int_{L=0}^{\infty} v_P N dL}_{nucleation} + \underbrace{\int_{L=0}^{\infty}\frac{d(n_P v_P)}{dt}dL}_{growth} \\ &= \frac{\rho_S}{M_S}\frac{\pi}{6}\left(R_N L_{crit}^3 + 3\underbrace{\int_{L=0}^{\infty} L^2 G\psi(L)dL}_{Int}\right) \end{aligned} \tag{13}$$

where v_P and n_P stands respectively for the solid volume per particles and the number of particles. The integral term *Int* is approximated, within the implicit resolution loop.

When a perfectly mixed drop is assumed (CSTR case), the macroscopic balance equations can be written as:

$$\begin{cases} \dfrac{\partial C_{Ce(NO_3)_3}}{\partial t} = -2 \times r_{app} \\ \dfrac{\partial C_{H_2C_2O_4}}{\partial t} = -3 \times r_{app} \\ \dfrac{\partial C_{solid}}{\partial t} = r_{app} \\ \dfrac{\partial C_{HNO_3}}{\partial t} = 6 \times r_{app} \end{cases} \tag{14a}$$

Table 3 – Mesh influence on the mean solid size predicted by the CSTR model.

	n				
	20	50	100	200	300
d_{43} (μm)	19.4	11.2	9.3	8.5	8.5

Otherwise (FDR model), the following governing equations are considered:

$$\begin{cases} \dfrac{\partial C_{Ce(NO_3)_3}}{\partial t} = -2 \times r_{app} \\ \dfrac{\partial C_{H_2C_2O_4,reactor}}{\partial t} = -3 \times r_{app} + k_x S(C_{H_2C_2O_4,feed} - C_{H_2C_2O_4,reactor}) \\ \dfrac{\partial C_{H_2C_2O_4,feed}}{\partial t} = -k_x S(C_{H_2C_2O_4,feed} - C_{H_2C_2O_4,reactor}) \\ \dfrac{\partial C_{solid}}{\partial t} = r_{app} \\ \dfrac{\partial C_{HNO_3}}{\partial t} = 6 \times r_{app} \end{cases} \quad (14b)$$

where the apparent mass-transfer coefficient k_xS is adjusted on the mixing kinetic predicted by the CFD simulation of Config. 2.

The system of differential-algebraic equations obtained from Eqs. (9), (13) and (14) is solved in a fully implicit scheme, using the DDASSL integrator, based the GEAR method (Petzold, 1982). Finally, given the significant differences in magnitude between variables ψ and C and the particles size L in the international system of units, the equations are solved in dimensionless form. The model is programmed in FORTRAN for Linux.

The number of discretization points, n, considered for the discretization of the PBE equation, was varied from 20 to 300, in order to study the mesh influence on the results. No significant effect is detected between $n = 200$ and $n = 300$ neither on the macroscopic variables such as supersaturation nor on the solid mean diameter d_{43} (see Table 3). The number of discretization points was therefore fixed to $n = 200$ for further calculations, which results in a running time of the order of one minute on a uniprocessor, or ten seconds on a quad core.

Simulations were all performed by combining the balance equations with the kinetic parameters given in Table 2, and the Davies model for the calculation of activity coefficient (see Section 2).

3.3.2. *Simulation results*

The evolutions of the supersaturation in the drop predicted by both the CSTR (immediate mixing of the reagents) and FRD (mixing limited by mass-transfer) models are compared in Fig. 8. As we can observe, mass transfer limitation (suggested by either sessile drops experiment or CFD simulation of mixing) results in a progressive increase and a slower consumption of the supersaturation in the reaction zone as compared to the CSTR case, and the maximum supersaturation is slightly lower. The predicted particle size is therefore higher than under CSTR assumption ($d_{43} = 20.9$ μm vs. 8.5 μm), due to a reduction of the apparent reaction rate.

Although it is not possible at this stage to compare the model predictions (on a single drop) to the particle size achieved in pulsed column (regarding the overall emulsion), it is interesting to note that the mean size of the neodymium and cerium oxalate particles reported by (Borda et al., 2011) varies from $d_{43} = 15$–20 μm, and $d_{43} = 20$–30 μm respectively, which is quite closed to the FRD value.

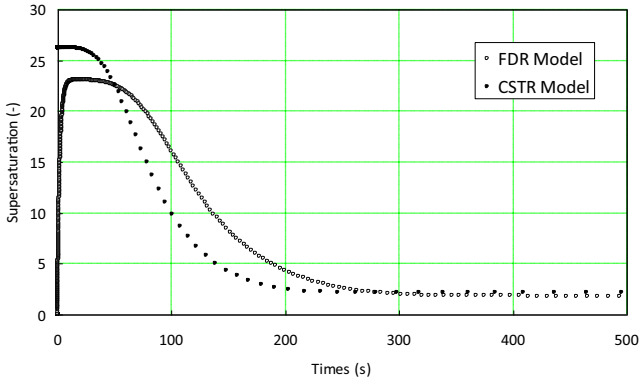

Fig. 8 – Supersaturation profile in the drop, comparison of the CSTR and FDR models predictions.

It should nevertheless be remembered that the aggregation phenomena was neglected in the model, while the occurrence of aggregation is suggested by SEM observations (see Fig. 9). Besides the possible occurrence of aggregation in the drops, the major uncertainty remains today the lack of kinetics data regarding cerium oxalate precipitation. As mentioned above (Section 2), the available kinetics data are relative to the neodymium system. They were measured using a high-speed mixer capable of achieving mixtures within times compatible with the measurement of nucleation kinetics (Bertrand-Andieu et al., 2004). However, given the stochastic nature of nucleation, the overall kinetic parameters are usually biased, or at least dependant of the mixing time (Zauner and Jones, 2000). Therefore, in order to investigate the uncertainty associated with kinetic data, the nucleation rate constant B_N was modified in the range −30% to +30%. The results regarding the apparent reaction rate r_{app} are illustrated in Fig. 10. When the nucleation rate is increased ($B_N = -30\%$), a large amount of particles is created, which rapidly consume the supersaturation. The apparent rate, which is mainly due to the growth rate contribution, increases therefore sharply, and vanishes quickly as well, thus resulting in small diameter particles ($d_{43} = 2.5$ μm). Conversely, when the nucleation rate is decreased ($B_N = +30\%$), the number of nuclei decreases as well, and larger particle size is achieved ($d_{43} = 31.3$ μm). Kinetic studies of the cerium oxalate system are underway, in order to overcome this uncertainty.

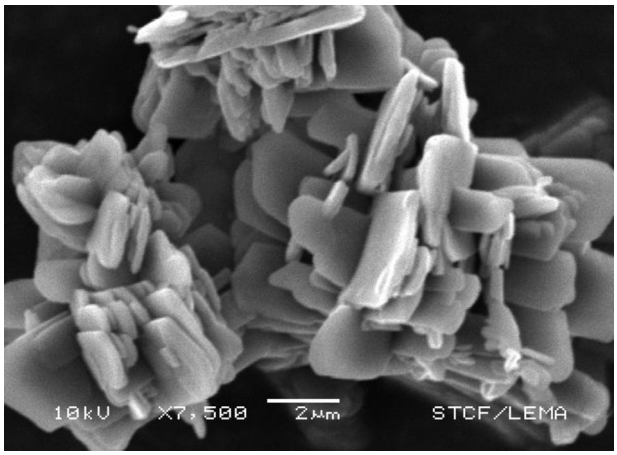

Fig. 9 – SEM pictures of cerium oxalate aggregates produced in pulsed column (Borda et al., 2011).

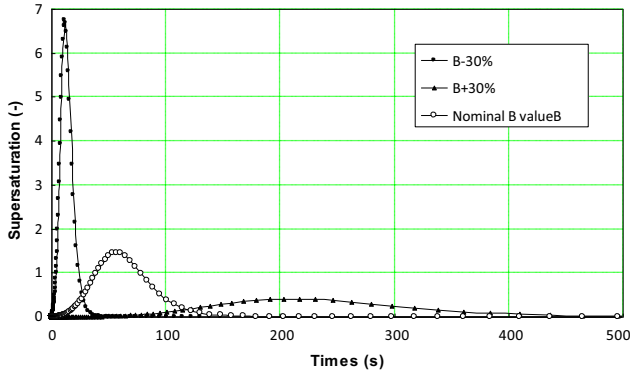

Fig. 10 – Apparent precipitation rate using the CSTR assumption – dependence on a ±30% uncertainty on kinetic data.

3.4. *Precipitation modeling inside a drop: coupled CFD + PBE simulations*

Beyond the mixing simulations presented in Section 3.2, some coupled CFD-PBE simulations were led using ANSYS-FLUENT. For the sake of comparison with the simplified approach, the same thermodynamic and kinetic models were considered, providing C++ user defined functions.

Several methods are available in the code for the PBE resolution. The "discrete method", DM, which requires important computational effort, is rarely used, since PBE has to be solved in each cell of the computational domain. It has however been used recently and successfully by Fernández Moguel et al. (2010) for the precipitation of barium carbonate in a fluidized bed, assuming 19 classes.

The Quadrature Method Of Moments method, QMOM, is much faster, since the PBE is transformed into a series of moment equations, which are used to approximate the particle size distribution (Marchisio et al., 2003).

QMOM simulations were performed to extend the model described Section 3.2 to the simulation of the precipitation in the flowing drop. The 6th first moments of the PSD were considered.

The simulation results regarding Config. 1 and Config. 2 are compared Fig. 11, which exhibit a qualitatively good agreement with respectively the CSTR and FRD models predictions. Additional work is nevertheless required to achieve better quantitative agreement between the simplified and the coupled-CFD approaches, especially regarding the evaluation

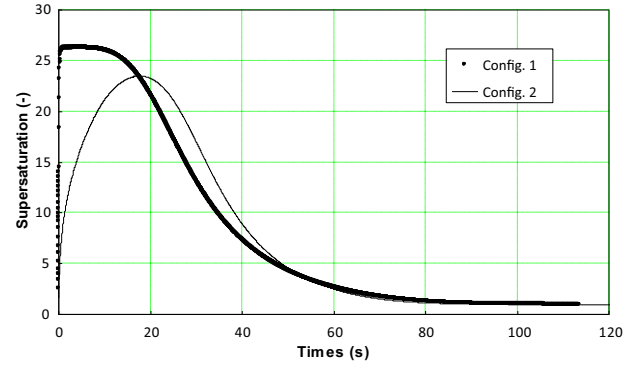

Fig. 11 – Initial conditions influence on the precipitation kinetics predicted by coupled CFD + PBE simulations using the QMOM model.

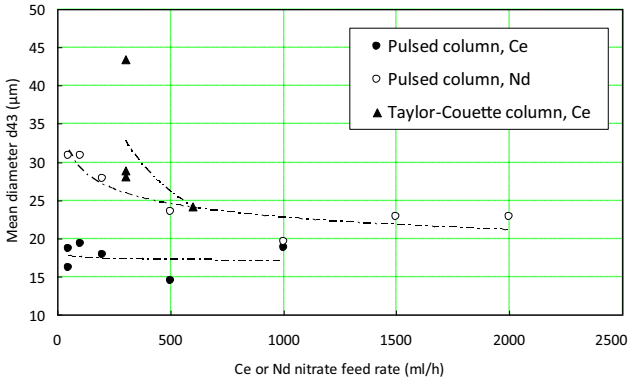

Fig. 12 – Particle size evolution with the column feed rate – fixed TPH flow-rate, fixed hydrodynamic conditions (pulsed intensity or rotor speed), fixed and identical oxalic over Ce or Nd ratio (1.7).

of the mass transfer resistance for the FRD and computational setup (time steps, PBE model and grid convergence, etc.).

4. Discussion: toward the industrial process modeling

The modeling of the precipitation process in emulsion in a pulsed column is a complicated task. In this aim, since the external hydrodynamic conditions at the drop boundaries interact with the precipitation, a two-scale modeling approach (column and drop) was considered and we chose to deal with these two scales separately.

For the first one a coupled CFD-PBE approach is currently developed (Amokrane et al., 2012) in order to characterize the drops population flowing in the apparatus, depending on the operating conditions. Thus, while the mean drop residence time and slip velocity are, to the first order, directly related to the column operating conditions, simulations of the drops population at the column scale, will allow the discretization of the device in a reasonable number of compartments, according to the drops coalescence frequency and their resulting chemical composition. Such compartmental modeling approach of the reactor, whose efficiency was demonstrated for the simulation of kinetic problems coupled to one-phase hydrodynamic solutions (Le Moullec et al., 2010; Bertrand et al., 2012), is indeed particularly convenient for the liquid–liquid flow prevailing in our process.

For the drop scale, a reaction engineering type model was proposed, which is intended, eventually, at the coupling with the "column level" description. CFD was used to study the mixing kinetics in a drop undergoing a straight downward motion, with a velocity typical of the one encountered in the pulsed column. The qualitative agreement achieved between the simplified model predictions and the CFD + PBE simulations confirms that the simplification of the process modeling by simplifying the hydrodynamic description at the drop scale is feasible. This approach is used to achieve relevant droplet's division in "reservoir" and "reactive" zones, and the evaluation of the related mass-transfer coefficients. It will now be applied for all typical boundary conditions (in terms of slip velocity type and magnitude) encountered in either the pulsed or the Taylor–Couette columns.

Beyond the possible evolution of the nuclear industry's needs in term of either production capacity or fuel composition, one of the challenges of emulsion process for

precipitation lies in the variability it offers regarding the oxalate morphology, and its related usage properties. Indeed, because the emulsion process is slightly dependent on the position of the reagents' feed lines, the proportion (or characteristic times) of either the nucleation, growth or aggregation process can be controlled individually. For instance, as illustrated Fig. 12, particle size can be easily tuned by changing the flow-rates (i.e. the drops residence time), etc.

A reliable and phenomenological model as the one currently developed would therefore be a powerful tool for the design and production of particles with controlled properties.

Notation

A	pulsation's amplitude (usually in mm)
A_N	kinetic parameter of the primary nucleation rate law ($m^{-3}\,s^{-1}$)
a	ion size constant
a_N	slope of the linearized nucleation rate N in the nucleation class ($m^{-3}\,s^{-1}$)
B_N	kinetic parameter of the primary nucleation rate law
b_N	constant of the linearized nucleation rate N in the nucleation class ($m^{-1}\,m^{-3}\,s^{-1}$)
C	molar concentration (usually $mol\,m^{-3}$ except in the expression of I in $mol\,l^{-1}$)
d	drop diameter (usually in mm)
d_{43}	mean particle diameter (usually in mm)
f	pulsation's frequency (s^{-1})
G	growth rate of the particles ($m\,s^{-1}$)
G_0	kinetic parameter of the growth rate law ($m\,s^{-1}$)
g	gravity ($m\,s^{-2}$)
I	ionic strength ($mol\,l^{-1}$)
K_{SP}	solubility product
k_xS	apparent mass transfer coefficient through the veil ($m^3\,s^{-1}$)
L	characteristic size of the particle (m)
M_S	molar weight of the solid phase ($kg\,mol^{-1}$)
N	nucleation rate for particles of size L ($m^{-1}\,m^{-3}\,s^{-1}$)
$\mathbf{N}$	Avogadro number (mol^{-1})
n	number of discretization points for the PBE
n_P	number of particles
Q	volumetric flow-rate (usually in $l\,h^{-1}$)
R_N	nucleation rate ($m^{-3}\,s^{-1}$)
r_{app}	apparent (macroscopic) reaction rate ($mol\,m^{-3}\,s^{-1}$)
s	supersaturation ratio, also designated as "supersaturation" for simplification
TPH	Tetra Propylene Hydrogen, the organic phase in the pulsed column (inert)
u_{ax}	slip velocity for drops undergoing an axial motion ($m\,s^{-1}$)
u_θ	tangential velocity (i.e. in the drop referential) ($m\,s^{-1}$)
v_P	volume of a solid particle (m^3)
z	charge number
$Eo = (g\Delta\rho d^2)/\sigma$	Eötvös number
$Re = (\rho u_{ax} d)/\mu$	drop Reynolds number

Symbols

Ψ	number particle distribution function ($m^{-3}\,m^{-1}$)
γ	activity coefficient
μ	TPH viscosity (Pa s)
ν	stoichiometric coefficient
ρ	TPH density ($kg\,m^{-3}$)
ρ_S	solid phase's density ($kg\,m^{-3}$)
σ	water/TPH interfacial tension ($N\,m^{-1}$)

Subscripts

crit	related to the nucleation class or crystal nuclei
eq	at equilibrium (achieved at steady-state in the column settler)
feed	related to the feed solution of the column or to the reservoir zone of the drop (FRD model)
load	related to the cation (Nd, Ce, etc.) nitrate solution
oxalic	related to the oxalic acid solution
reactor	related to the reaction zone of the drop (FRD model)
solid	related to the solid phase

References

Amokrane, A., Charton, S., Lamadie, F., Becker, J., Klein, J.-P., Puel, F., 2012. Study of the dispersed phase behavior in a pulsed column for oxalate precipitation in an emulsion. In: Proceedings of the 9th Int. Conf. on CFD in the Minerals and Process Industries, CSIRO, Melbourne, Australia, 10–12 December.

Auchapt, P., Ferlay, A., 1983. Vortex flow apparatus for making a precipitate. EPO Patent EP0072737.

Andrieu, M., 1999. Etude cinétique de la nucléation et de la croissance cristalline au cours de la précipitation oxalique dans l'industrie nucléaire. Ph.D. Institut National Polytechnique de Lorraine.

Bandyopadhyaya, R., Kumar, R., Gandhi, K.S., Ramkrishna, D., 1997. Modeling of precipitation in reverse micellar systems. Langmuir 13, 3610–3620.

Bertrand-Andieu, M., Plasari, E., Baron, P., 2004. Determination of nucleation and crystal growth kinetics in hostile environment – application to the tetravalent uranium oxalate. Can. J. Chem. Eng. 82, 930–938.

Bertrand, M., Plasari, E., Lebaigue, O., Baron, P., Lamarque, N., Ducros, F., 2012. Hybrid LES-multizonal modelling of the uranium oxalate precipitation. Chem. Eng. Sci. 77, 95–104.

Borda, G., Duhamet, J., Gandi, F., Lanoë, J.-Y., 2008. Method and device for precipitating a solute. Patent WO 2008/025823.

Borda, G., Brackx, E., Boisset, L., Duhamet, J., Ode, D., 2011. Use of a pulsed column contactor as a continuous oxalate precipitation reactor. Nucl. Eng. Des. 241, 809–814.

Bromley, L.A., 1973. Thermodynamic properties of strong electrolytes in aqueous solution. AIChE J. 19 (2), 313–320.

Chung, D.Y., Kim, E.-H., Lee, E.-L., Yoo, J.-H., 1998. Solubility of rare earth oxalate in oxalic and nitric acid media. J. Ind. Eng. Chem. 4 (4), 277–284.

Cameirão, A., David, R., Espitalier, F., Gruy, F., 2008. Effect of precipitation conditions on the morphology of strontium molybdate agglomerates. J. Cryst. Growth 310, 4152–4162.

Chang, T.P., 1987. Cerium Oxalate Precipitation, Dupont de Nemours Report DP-1723/DE87 007832. Savannah River Laboratory.

Clift, R., Grace, J.R., Weber, M.E., 1978. Bubbles Drops and Particles. Academic Press, New York (Chapter 3).

Davey, R., Hilton, A.M., Garside, J., 1997. Crystallization from oil in water emulsions: particle synthesis and purification material. Chem. Eng. Res. Des. 75 (A), 245–251.

Davies, C.W., 1938. Interpretation of activity measurements. J. Am. Ceram. Soc. 58, 2093.

Espitalier, F., Biscans, B., Authelin, J.-R., Laguerie, C., 1997. Modelling of the mechanism of spherical grains obtained by the quasi-emulsion crystallization process. Chem. Eng. Res. Des. 75 (A2), 257–267.

Fang, W.-F., Yeh, S.I., Chen, Y.T., Yang, J.T., 2011. Coalescence and mixing of droplets with identical and distinct surface tensions on a wettability gradient surface. Seattle, USA, October 2–6. Proceedings 15th Int. Conf. Miniaturized Systems for Chemistry and Life Sciences.

Fernández Moguel, L., Muhr, H., Dietz, A., Plasari, E., 2010. CFD simulation of barium carbonate precipitation in a fluidized bed reactor. Chem. Eng. Res. Des. 88, 1206–1216.

Groß-Hardt, E., Slusanschi, E., Bücker, H.M., Pfennig, A., Bischof, C.H., 2008. Practical shape optimization to a levitation device for single droplets. Optim. Eng. 9, 179–199.

Ilievski, D., Rudman, M., Metcalfe, G., 2001. The separate roles of shear rate and mixing on gibbsite precipitation. Chem. Eng. Sci. 56, 2521–2530.

Khalil, A., Puel, F., Cosson, X., Gorbatchev, O., Chevalier, Y., Galvan, J.-M., Rivoire, A., Klein, J.P., 2012. Crystallization-in-emulsion process of a melted organic compound: in situ optical monitoring and simultaneous droplet and particle size measurement. J. Cryst. Growth 342 (1), 99–109.

Lalleman, S., Bertrand, M., Plasari, E., Sorel, C., Moisy, P., 2012. Determination of the Bromley contributions to estimate the activity coefficient of neodymium electrolytes. Chem. Eng. Sci. 77, 185–189.

Le Moullec, Y., Gentric, C., Potier, O., Leclerc, J.P., 2010. Comparison of systemic, compartmental and CFD modelling approaches: application to the simulation of a biological reactor of wastewater treatment. Chem. Eng. Sci. 65, 343–350.

Marcant, B., 1992. Méthodologie d'analyse d'un système de precipitation soumis à l'influence des conditions de mélange: cas de l'oxalate de calcium. Ph.D. INPL.

Marchisio, D.L., Barresi, A.A., 2003. CFD simulation of mixing and reaction: the relevance of micro-mixing model. Chem. Eng. Sci. 58, 3579–3587.

Marchisio, D.L., Virgil, R.D., Fox, R.O., 2003. Quadrature method of moments for aggregation-breakage processes. J. Colloid Interface Sci. 258, 322–334.

Medal, A., Picard, R., Charton, S., Puel, F., Borda, G., 2010. Etude de la precipitation oxalique dans une goutte et premières mdélisations. In: Proceeding of CRISTAL 6, Récents Progrès en Génie des Procédés, 99, SFGP, Paris.

Muhr, H., David, R., Villermaux, J., Jezequel, P.H., 1996. Crystallization and precipitation engineering: solving population balcance in the case of precipitation of silver bromide crystal with high primary nucleation rates by using the first order upwind differentiation. Chem. Eng. Sci. 51 (2), 309–319.

Nemri, M., Climent E., Charton, S., Lanoë, J.-Y., Ode, D., 2012. Experimental and numerical investigation on mixing and axial dispersion in Taylor–Couette flow patterns, Chem. Eng. Res. Des., http://dx.doi.org/10.1016/j.cherd.2012.11.010, in Press.

Petzold, L.R., 1982. A Description of DDASSL: A Differential-Algebraic System Solver. Tech. Rep. SAND82-8637.

Picard, R., 2012, Contribution à l'étude de la mouillabilité dans une colonne pulse dédiée à la fabrication d'un précipité. Ph.D. Ecole Centrale Paris, tel-00711473.

Pontisso, E.-A., Borda, G., Charton, S., Teychéné, S., Biscans, B., 2011. Precipitation en emulsion: mise en evidence et etude du rôle de l'interface sur la cinétique. In: Récents Progrès en Génie des Procédés, 101, SFGP, Paris.

Qamar, S., Ashfaq, A., Warnecke, G., Angelov, I., Elsner, M.P., Seidel-Morgenstern, A., 2007. Adaptative high-resolution schemes for multidimensional population balances in crystallisation process. Comput. Chem. Eng. 31, 1296–1311.

Saboni, A., Alexandrova, S., Gourdon, C., 2004. Détermination de la traînée engendrée par une sphère fluide en translation. Chem. Eng. J. 98, 175–182.

Ståhl, M., Rasmuson, A.C., 2009. Towards predictive simulation of single feed semibatch reaction crystallization. Chem. Eng. Sci. 64, 1559–1576.

Torbacke, M., Rasmuson, A.C., 2001. Influence of different scales of mixing in reaction crystallisation. Chem. Eng. Sci. 56, 2459–2473.

Zauner, R., Jones, A.G., 2000. Determination of nucleation, growth, agglomeration and disruption kinetics from experimental precipitation data: the calcium oxalate system. Chem. Eng. Sci. 55, 4219–4232.